Available online at www.sciencedirect.com
ScienceDirect
Journal of Theoretical Biology 242 (2006) 801–817
Journal of Theoretical Biology
www.elsevier.com/locate/yjtbi

Modeling the mechanism of metabolic oscillations in ischemic cardiac myocytes

M. Saleet Jafri[a,b,*], Malgorzata Kotulska[c]

[a]Department of Bioinformatics and Computational Biology, George Mason University, Manassas, VA 20110, USA
[b]Medical Biotechnology Center, University of Maryland Biotechnology Institute, Baltimore, MD 21201, USA
[c]Department of Biomedical Engineering and Instrumentation, Wroclaw University of Technology, 50-370 Wroclaw, Poland

Received 14 June 2005; received in revised form 10 April 2006; accepted 10 May 2006
Available online 19 May 2006

Abstract

Oscillations in energy metabolism have been observed in a variety of cells under metabolically deprived conditions such as ischemia. In cardiac ventricular myocytes these metabolic oscillations may cause oscillations in the action potential duration, creating the potential for cardiac arrhythmias during ischemia (O'Rourke, 2000). A mathematical model of the mechanism behind metabolic oscillations is developed here. The model consists of descriptions of the mitochondrial components that regulate mitochondrial membrane potential (Ψ), mitochondrial inorganic phosphate concentration, mitochondrial magnesium concentration, and cellular NADH and NAD^+ concentrations. Using parameters from the experimental literature, the model produces physiological values for these both under normoxic (steady state) and ischemic (oscillatory) conditions. The model includes the mitochondrial inner membrane anion channel (IMAC), the centum picosiemen channel (mCS), the phosphate carrier (PIC), and the respiration driven proton pumps. The model suggests that these are the essential components for producing oscillations with mCS essential for the rapid depolarization, PIC for the recovery from depolarization, and IMAC for the slow depolarization between depolarization peaks. A decrease of the inner membrane potential due to ischemia or experimental conditions seems to be a triggering factor for the oscillations. The model simulates the experimental observations that high levels of mitochondrial ADP and ATP abolish the oscillations, as does inhibition of electron transport. The model makes predictions on the influence of pH and magnesium levels on metabolic oscillations.

Keywords: Metabolic oscillations; Ischemia; Heart; Computer model

1. Introduction

Oscillations in mitochondrial energy metabolism, during conditions of metabolic stress, such as ischemia or substrate deprivation, have been observed in isolated cardiac mitochondria (Gooch and Packer, 1971; Gooch and Packer, 1974), cardiac myocytes (O'Rourke et al., 1994), respiratory neurons (Mironov and Richter, 2001), rat brain cortical neurons (Vergun et al., 2003, 2004) and yeast (Lloyd et al., 2002). These have been measured by three different methods: fluctuations of metabolite concentrations in metabolically impaired isolated mitochondria (Gooch and Packer, 1971), fluctuations in the autofluorescence of FAD whose redox state is tightly coupled to that of NADH (Romashko et al., 1998) and ATP-dependent ionic currents in ischemic cardiac myocytes (O'Rourke et al., 1994). In cardiac ventricular myocytes, the fluctuations in the sarcolemmal ATP-sensitive K^+ current are of clinical interest since activation of this current leads to shortening of the action potential which might lead to re-entrant arrhythmias. The metabolic oscillations are accompanied by oscillations in the inner mitochondrial membrane potential as measured by TMRE fluorescence (Romashko et al., 1998). Flavoprotein fluorescence is often used to experimentally measure metabolic oscillations (O'Rourke, 2000). The measurements made by this author show increased fluorescence during oxidation

*Corresponding author. Department of Bioinformatics and Computational Biology, George Mason University, 10900 University Blvd, MSN 5B3, Manassas, VA 20110, USA. Fax: +703 993 8401.
E-mail address: sjafri@gmu.edu (M. Saleet Jafri).

0022-5193/$ - see front matter © 2006 Elsevier Ltd. All rights reserved.
doi:10.1016/j.jtbi.2006.05.007

of NADH, i.e. conversion of NADH to NAD^+ as indicated by the addition of flavoprotein-oxidizing compounds such as Diazo. During the observed metabolic oscillations, depolarization of Ψ was accompanied by oxidation of NADH or an increase of flavoprotein fluorescence.

A number of hypotheses have been proposed to explain metabolic oscillations. An early explanation was that metabolic oscillations resulted from glycolytic oscillations (O'Rourke et al., 1994) similar to the phenomenon observed in yeast and bovine heart extracts (Frenkel, 1968; Ghosh and Chance, 1964). The same group of researchers ruled out this explanation because agents that block mitochondrial inner membrane anion channels (IMACs) reversibly block metabolic oscillations (O'Rourke, 2000). Specifically, the benzodiazepine PK11195 (at high concentration), amiodarone, amitriptyline, and propranolol, that block the mitochondrial inner membrane low conductance channel, reversibly terminate the oscillations. PK11195 has also been shown to block two other IMAC, namely, the multiple conductance channel (MCC) and the mitochondrial centum-picosiemen (mCS) channel (Kinnally et al., 1993). Additional evidence against the glycolytic hypothesis comes from the fact that oscillations could be observed in isolated mitochondria from various cells (Bernardini et al., 1982; Gooch and Packer, 1971, 1974; Vergun et al., 2003) where no glycolytic enzymes are likely to be present.

The hypothesis that the reactive oxygen species (ROS) play an important role in the oscillation in mitochondrial membrane potential and redox state was presented recently by Aon and co-workers (Aon et al., 2003). In their experiments, a single laser flash triggered synchronized and self-sustaining oscillations in Ψ, ADH, and ROS. The oscillations were inhibited by blockers of the electron transport chain and by pre-incubation with a ROS scavenger. They assume that IMAC–LCC is voltage and ROS sensitive and hence is crucial for the oscillations. However, this model does not explain the effect of Ca^{2+} and adenine nucleotides on oscillations as observed by Vergun and colleagues (2004). Furthermore, there are two uncertainties about the assumptions of the model of Cortassa and co-workers and how they are supported by experimental observations. First, the model does not account for the experimental finding that the permeablity transition pore (PTP) opens in response to increased ROS concentration. In fact, Brady and co-workers (2004) observed that laser generation of ROS, the same procedure used by Cortassa et al. (2004), results in a wave of depolarization due to opening of PTP. Cortassa and co-workers failed to test if PTP was involved in the oscillations due to laser-generated ROS formation.

In contrast, earlier experimental work by Cortassa and co-workers (2003) showed that PTP was not involved in metabolic oscillations resulting from metabolic stress. PTP opening causes the redistribution of calcein, a fluorescent probe, from the mitochondrial matrix to the cytoplasm. They observed no movement of calcein out of the mitochondria in these experiments. Vergun and colleagues (2003) also observed no movement of calcein during metabolic oscillations and that application of cyclosporin A, a PTP inhibitor, did not terminate the oscillations. In summary, it is clear that the oscillations observed by these two groups do not involve PTP, however, it is not clear why PTP will not open with the large increases in ROS ($>100\,\mu M$) suggested by the model by Cortassa and co-workers.

Secondly, the model by Cortassa and co-workers assumes that IMAC is activated by ROS for which there is no experimental evidence. In his thorough review, Beavis (1992) describes the regulation by several factors including Mg^{2+} and H^+, but makes no reference to ROS.

We propose an alternative mechanism for oscillations in Ψ, NADH, and ATP production during metabolic stress that accounts for the regulation of oscillations by Ca^{2+} and adenine nucleotides. In the model ROS is not needed for oscillations to appear, but fluctuations in ROS generation are possible during oscillations.

2. The model

This manuscript presents a model (Fig. 1) of the mitochondria consisting of dynamic equations for the membrane potential across the mitochondrial inner membrane (Ψ) and the mitochondrial matrix inorganic phosphate concentration ($[P_i]_m$). The model includes descriptions of the current that restores Ψ consisting primarily of the respiration-driven proton pumps (I_{resp}), the current generated by F_1F_0-ATPase (I_{ATP}), the phosphate carrier flux (J_{PIC}), the low-conductance IMAC current (I_{IMAC}), mCS current (I_{mCS}), buffering of $[P_i]_m$ by the mitochondrial matrix magnesium and mitochondrial matrix calcium, and buffering of the mitochondrial matrix magnesium concentration ($[Mg^{2+}]_m$) by mitochondrial matrix ATP and ADP. The model also includes several assumptions to isolate the salient mechanisms behind the oscillations: (1) Mg^{2+} and P_i binding is in rapid equilibrium (i.e. the binding reaction if fast compared to the other processes included in the model; (2) Ca^{2+} and P_i binding is in rapid equilibrium; (3) Mg^{2+} binding to ATP and ADP is in rapid equilibrium; (4) the mitochondrial pH, matrix [ADP], and matrix [ATP] remain constant over the course of an oscillation although the effect of their different concentrations is tested. This assumption simplifies the model and the fundamental mechanisms responsible for oscillations are not obscured; (5) P_i is the only charge carrier considered for the anion channel currents. The parameters for the model are given in Table 1 along with the reference to the experimental literature from where they were obtained.

The mitochondrial inner membrane potential (Ψ) is maintained primarily by the action of respiration-driven proton pumps (I_{resp}) that use the energy contained in NADH and $FADH_2$ to pump hydrogen ions (H^+) across

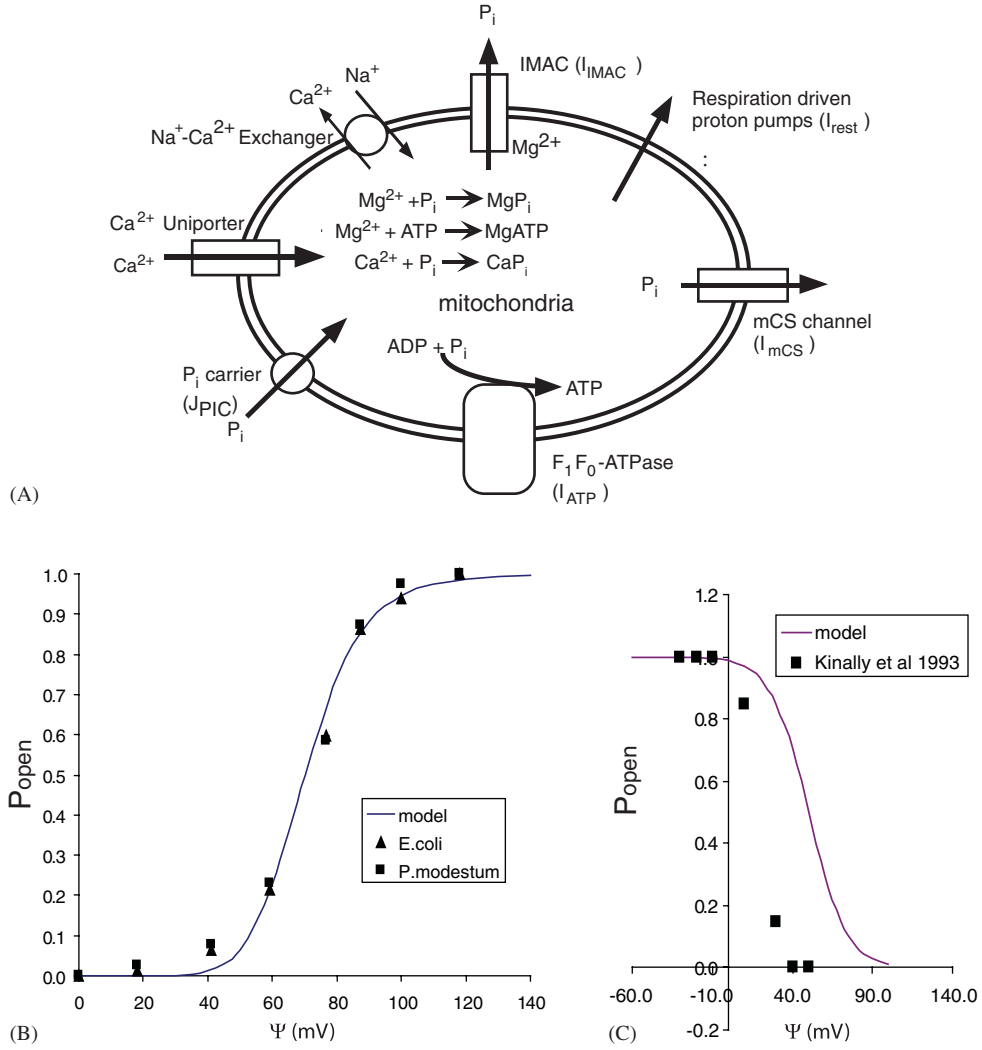

Fig. 1. (A) Schematic diagram of mitochondrial components involved in metabolic oscillations; (B) the model formulation for the F_1F_0-ATPase (Eq. (2)) compared with the experimental data from Kaim and Dimroth (1999); and (C) the model formulation of the IMAC mCS compared to the experimental data of Kinally and co-workers (1993).

the mitochondrial membrane out of the mitochondrial matrix. This process involves the electron transport chain whose dependence on NADH and voltage and is described by

$$I_{resp} = \frac{[\mathrm{NADH}]_m}{(K_{resp} + [\mathrm{NADH}]_m)} \frac{(\psi - E_{resp})}{R_{resp}}, \quad (1)$$

where the first term represents the NADH dependence as described by Hagedorn and co-workers (2004) and the second term reflects current of the H^+ ions working against the membrane potential. The parameter E_{resp} is the equilibrium potential for the restorative processes and R_{resp} is the "effective resistance" for the restorative processes. The mitochondrial matrix concentration is $[\mathrm{NADH}]_m$ and K_{rest} is Michaelis constant for the NADH dependence. Under normal conditions E_{rest} is 258 mV, and under metabolically deprived or ischemic conditions it is reduced to 190 mV to reflect the decrease in electron transport resulting from diminished oxygen availability (Berkich et al., 2003).

The F_1F_0-ATPase or ATP synthase uses the membrane potential to generate ATP from ADP and P_i by allowing H^+ ions to flow into the mitochondria. The production of ATP by the F_1F_0-ATPase depends mainly on Ψ as observed by Kaim and Dimroth (1999) in bacteria. Furthermore Kain and Dimroth in bacteria and Berkich and co-workers (1991) in heart mitochondria both measured a sigmoid dependence of ATP production on mitochondrial membrane potential. An equation for I_{ATP} in μA was developed to describe their data

$$I_{atp} = V_{\max}^{ATP} \frac{\Psi^8}{\left(K_m^{ATP}\right)^8 + \Psi^8}, \quad (2)$$

where V_m^{ATP} is the maximal current generated by the ATP synthase, and K_m^{ATP} is the membrane potential that yields half-maximal ATP production current. When Ψ is above 110 mV the voltage dependence saturates consistent with experimental findings (Knox and Tsong, 1984).

Table 1
Model parameters

Parameter	Definition	Value (reference)
E_{rest}	Restorative process resting potential—normoxia	258 mV[a]
	Restorative process resting potential—ischemia	190 mV[b]
R_{rest}	NADH-dependent resistance for restorative process	7.40 MΩ*
$V_{\max}^{ATP}$	Maximal ATPase flux	0.4045 mM/s[c,d]
K_m^{ATP}	Membrane potential for half-maximal ATPase current	70.0 mV[e]
v_f	Phosphate carrier maximal P_i uptake rate	1.984 mM/s[f]
$K_{Pi,i}$	Phosphate carrier cytosolic P_i dissociation constant	1.6 mM[f]
v_b	Phosphate carrier maximal P_i efflux rate	1.984 mM/s[g,*]
$K_{Pi,m}$	Phosphate carrier mitochondrial P_i dissociation constant	11.0 mM[f]
$K_{OH,m}$	Phosphate carrier mitochondrial OH binding constant	32.84 nM[f]
$K_{OH,i}$	Phosphate carrier cytosolic OH binding constant	81.83 nM[f]
pH_m	Mitochondrial matrix pH—normoxic	7.5[h]
	Mitochondrial matrix pH—ischemic	7.1[h]
pH_i	Extramitochondrial pH—normoxic	7.1[h]
	Extramitochondrial pH—ischemic	7.0[h]
$[OH]_m$	Mitochondrial matrix OH concentration	$10^{-(14-pHm)}$ M[i]
$[OH]_i$	Extramitochondrial OH concentration	$10^{-(14-pHi)}$ M
$[P_i]_i$	Normoxic cytosolic P_i concentration	2.78 mM[g]
	Ischemic cytosolic P_i concentration	8.34 mM[j]
$[H^+]$	Normoxic H^+ matrix concentration	$10^{-7.2}$ M[i]
G_{IMAC}	Maximal IMAC conductance	0.1125 nS[k]
R	Ideal gas constant	8.314 J mol K
T	Absolute temperature	310 K
Z	Valence of Ca^{2+}	2
F	Faraday's constant	96500 C mol
K_{H1}	IMAC H^+ binding constant	1.58×10^{-7} M[l]
K_{H2}	IMAC H^+ binding constant for Mg^{2+} binding	1.29×10^{-7} M[l]
K_{Mg}	IMAC Mg^{2+} constant	8.2×10^{-6} M[l]
G_{mCS}	Maximal mCS channel conductance	2.645 nS[m]*
C_m	Mitochondrial membrane capacitance	5.2 nf[n]
W	Mitochondrial matrix volume	24.7 pl[n,o]
K_{MgPi}	Mg/P_i dissociation constant	1.176 mM[g]
K_{CaPi}	Ca/P_i dissociation constant	2.857 mM[g]
$[Mg^{2+}]_{total}$	Total mitochondrial matrix Mg^{2+} concentration	42.8 mM[g]
$[Ca^{2+}]_{total}$	Total mitochondrial matrix Ca^{2+} concentration	12.7 mM[g]
K_{MgATP}	Mg/ATP dissociation constant	0.017 mM[g]
$[ATP]_m$	Mitochondrial matrix free ATP concentration	0.44 mM[g]
K_{MgADP}	Mg/ADP dissociation constant	0.282 mM[g]
$[ADP]_m$	Mitochondrial matrix free ADP concentration	2.49 mM[g]
K_{MgAMP}	Mg/AMP dissociation constant	500.0 mM[g]
$[AMP]_m$	Mitochondrial matrix free AMP concentration	2.5 mM[g]
K_{MgGTP}	Mg/GTP dissociation constant	0.50 mM[g]
$[GTP]_m$	Mitochondrial matrix free GTP concentration	0.44 mM[g]
$[B]_{total}$	Total mitochondrial matrix Mg^{2+} buffer concentration	12.8 mM[g]
K_{MgB}	Mg/B dissociation constant	0.22 mM[g]
K_{NAD}	NAD consumption rate constant	0.9 s[p,*]
$[Ca^{2+}]_i$	Extramitochondrial free Ca^{2+} concentration	0.0001 mM[h]
P_{Ca}	Uniporter Ca^{2+} permeability	2.27×10^{-16} cm s[q,r,*]
α_m	Mitochondrial Ca^{2+} activity coefficient	0.2[q,*]
α_i	Cytosolic Ca^{2+} activity coefficient	0.341[q,*]
V_{nc}	Na^+–Ca^{2+} exchanger maximal velocity	0.2 mM/s[r,*]
K_{Na}	Na^+–Ca^{2+} exchanger Na^+ affinity	9.4 mM[s]
K_{Ca}	Na^+–Ca^{2+} exchanger Ca^{2+} affinity	4.54 mM[s]
$[Na^+]_i$	Extramitochondrial Na^+ concentration	10.0 mM[n]
$[Na^+]_i$	Mitochondrial matrix Na^+ concentration	5.0 mM[t]
k_{DH}	Maximal rate of NADH production	35.1 mM/s[u,*]
K_{mN}	$[NAD^+]_m/[NADH]_m$ ratio that gives half-maximal NADH production	100[v]
p_{DH}	Cooperativity factor for NADH production	0.8[v]
$K_{m,CI}$	Complex I NADH affinity	0.08 mM[w]
β	Mitochondrial matrix calcium buffering factor	0.003[x]
$V_{ADP\text{-}trans}$	ADP/ATP translocase maximal velocity for ADP uptake	0.31 s[u]
$K_{ADF\text{-}trans,m}$	Mitochondrial ADP/ATP translocase ADP binding constant	0.03 mM[u]
$K_{ADP\text{-}trans,I}$	Extramitochondrial ADP/ATP translocase ADP binding constant	0.003 mM[u]

Table 1 (*continued*)

Parameter	Definition	Value (reference)
$[ADP]_I$	Extramitochondrial ADP concentrations	0.014 mM normoxic 0.0 mM, 0.1 mM[y]
$V_{ATP\text{-}trans}$	ADP/ATP translocase maximal velocity for ATP uptake	3.01 s[u]
$K_{ATF\text{-}trans,m}$	Mitochondrial ADP/ATP translocase ATP binding constant	0.110 mM[u]
$K_{ATF\text{-}trans,I}$	Extramitochondrial ADP/ATP translocase ATP binding constant	0.110 mM[u]
$[ATP]_i$	Extramitochondrial ADP concentrations	0.5 mM normoxic 0.0 mM, 0.1 mM[y]

The model parameters were obtained from the following experimental references:

*Value fit to data.

[a]Skárka and Ostádal (2002).
[b]DiLisa et al. (1995).
[c]Taegtmeyer et al. (1998).
[d]Hochachka (1999).
[e]Kaim and Dimroth (1999).
[f]Stappen and Krämer (1994).
[g]Corkey et al. (1986).
[h]Nyguen and Jafri (2005).
[i]Sato et al. (1995).
[j]Armiger et al. (1995).
[k]Kinnally et al. (1992).
[l]Beavis and Powers (1989).
[m]Murphy et al. (1998).
[n]Bers (2001).
[o]Scalettar et al. (1991).
[p]Livingston et al. (1996).
[q]Kirichok et al. (2004).
[r]Trollinger et al. (2000).
[s]Wingrove and Gunter (1986).
[t]Donoso et al. (1992).
[u]Barbour and Chan (1981).
[v]Korzeniewski and Zoladz (2001).
[w]Hagedorn et al. (2004).
[x]Magnus and Keizer (1997).
[y]Vergun et al. (2004).

The phosphate carrier carries phosphate into the mitochondria in one of three electro-neutral transport modes: P_i/P_i counter-transport, P_i/OH^- counter-transport, or P_i/H^+ co-transport (Stappen & Krämer, 1994). The carrier is a bi-directional P_i/OH symporter that forms a ternary complex of P_i, OH, and the carrier. Therefore, the model is based on reversible Michaelis–Menten kinetics that involves two ternary complex with a random order of addition of substrates resulting in simultaneous transport of the two substrates. The carrier X has the kinetic scheme

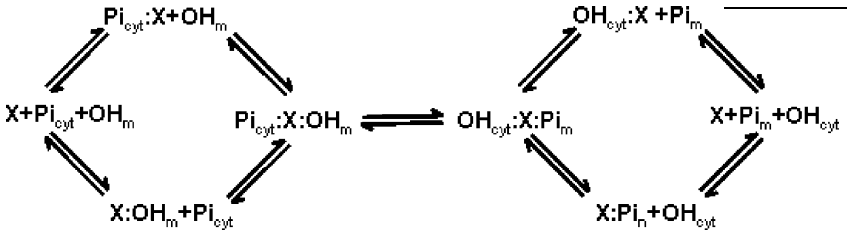

in which Pi and OH can bind reversibly on either the cytoplasmic or mitochondrial side of the carrier in any order. When a Pi and an OH are bound on opposite sides of the carrier, a translocation can occur (middle). A mathematical description for this mechanism has been derived as follows:

$$J_{PIC} = \frac{v_{Pi,f}\frac{[P_i]_i[OH]_m}{K_{Pi,i}K_{OH,m}} - v_{Pi,b}\frac{[P_i]_m[OH]_i}{K_{Pi,m}K_{OH,i}}}{1+\frac{[P_i]_i}{K_{Pi,i}}+\frac{[OH]_m}{K_{OH,m}}+\frac{[P_i]_i[OH]_m}{K_{Pi,i}K_{OH,m}}+\frac{[P_i]_m}{K_{Pi,m}}+\frac{[OH]_i}{K_{OH,i}}+\frac{[P_i]_m[OH]_i}{K_{Pi,m}K_{OH,i}}}, \quad (3)$$

where v_f is the maximal uptake rate, v_b is the maximal efflux rate, K_f is the cytosolic P_i dissociation constant, $[P_i]_i$

is the extramitochondrial P_i concentration, K_{OH} is the OH binding constant, $[OH]_m$ is the mitochondrial matrix OH concentration, $[OH]_i$ is the extramitocondrial OH concentration, $[P_i]_m$ is the mitochondrial matrix P_i concentration, and K_b is the mitochondrial matrix P_i dissociation constant measured by Stappen and Krämer (1994). When there is nonzero net P_i transport, i.e. the uptake and efflux rates are unequal, P_i/OH^- counter-transport is most likely (Stappen and Krämer, 1994). The resting $[P_i]_i$ is 2.78 mM under normoxic conditions (Corkey et al., 1986) and increases under ischemic conditions to 8.34 mM. This is well within the range of approximately 2.0 mM in well-oxygenated heart up to 30.0 mM during prolonged ischemia described by van der Velden and co-workers (2001).

The low-conductance IMAC has a single channel conductance of 15 pS. It is activated by low pH and inhibited by Mg^{2+} (Beavis, 1992; Kinnally et al., 1992). The IMAC current is described by

$$I_{IMAC} = P_{IMAC} G_{IMAC} (\Psi - E_{Pi}), \tag{4}$$

where G_{IMAC} is the maximal mitochondrial IMAC conductance. The reversal potential is given by the Nernst potential of P_i

$$E_{Pi} = \frac{RT}{zF} \ln \frac{[P_i]_{cyt}}{[P_i]_m}, \tag{5}$$

where R is the ideal gas constant, T is the absolute temperature, $z = -2$ is the assumed average charge on phosphate, and F is Faraday's constant. The -2 charge is an average between the -3, -2, and -1 charges possible for phosphate. The regulation of the open probability of the IMAC by mitochondrial matrix pH and matrix Mg^{2+} concentration has been described by Beavis and co-workers (1989) as

$$P_{IMAC} = \frac{1}{\left(1 + \frac{[H^+]}{K_{H_1}}\right)\left(1 + \frac{[Mg^{2+}]_m [H^+]}{K_{Mg}(K_{H_2} + [H^+])}\right)}, \tag{6}$$

based on their experimental findings, where k_{H1} and k_{H2} are the binding constants for H^+ to the channel and k_{Mg} is the binding constant for Mg^{2+} to the channel.

The mCS channel is a voltage-dependent anion channel with a single channel conductance of 110 pS (Murphy et al., 1998). It is blocked by the benzodiazepine PK11195 (Kinnally et al., 1993). The ionic current can be described by

$$I_{mCS} = P_{mCS} G_{mCS} (\Psi - E_{Pi}), \tag{7}$$

where G_{mCS} is the maximal mCS channel conductance. The open probability (P_{mCS}) has been observed experimentally by Kinnally and co-workers (1993) and, based on their data, we approximate its voltage dependence by the function

$$P_{mCS} = \frac{\exp\left\{\frac{5.0 \cdot (50.0 - \Psi)}{58.0}\right\}}{1.0 + \exp\left\{\frac{5.0 \cdot (50.0 - \Psi)}{58.0}\right\}}. \tag{8}$$

The model also included a description of mitochondrial Ca^{2+} handling and can explore the effect of Ca^{2+} on the oscillations. Calcium enters the mitochondria by Ca^{2+} uniporter which has been characterized experimentally by Kirichok and co-workers (2004) and described mathematically by Nguyen and Jafri (2005) as

$$J_{uni} = P_{Ca} \frac{z_{Ca} \Psi F}{VRT} \frac{\alpha_m [Ca^{2+}]_m \exp\left[\frac{-z_{Ca} \Psi F}{RT}\right] - \alpha_i [Ca^{2+}]_i}{\exp\left[\frac{-z_{Ca} \Psi F}{RT}\right] - 1}. \tag{9}$$

Ca^{2+} is extruded from the mitochondria by the Na^+/Ca^{2+} exchanger which improves upon the formulation by Nguyen and Jafri (2005) by adding the dependence on the mitochondrial membrane potential

$$J_{nc} = \frac{v_{nc}\left[e^{0.5\Psi F/RT}\frac{[Na^+]_i^3 [Ca^{2+}]_m}{K_{Na}^3 K_{Ca}} - e^{-0.5\Psi F/RT}\frac{[Na^+]_m^3 [Ca^{2+}]_i}{K_{Na}^3 K_{Ca}}\right]}{1 + \frac{[Na^+]_i^3}{K_{Na}^3} + \frac{[Ca^{2+}]_m}{K_{Ca}} + \frac{[Na^+]_i^3 [Ca^{2+}]_m}{K_{Na}^3 K_{Ca}} + \frac{[Na^+]_m^3}{K_{Na}^3} + \frac{[Ca^{2+}]_i}{K_{Ca}} + \frac{[Na^+]_m^3 [Ca^{2+}]_i}{K_{Na}^3 K_{Ca}}}, \tag{10}$$

where v_{nc} is the exchanger rate, $[Na^+]_i$ is the extramitochondrial sodium concentration, $[Na^+]_m$ is the mitochondrial matrix sodium concentration, K_{Na} is the binding constant for sodium and K_{Ca} is the binding constant for calcium.

Buffering with P_i and other molecules is modeled as rapid buffering and simulated by Magnus–Keizer buffering factor (Magnus and Keizer, 1997). In the mitochondrial matrix, P_i binds Ca^{2+} and Mg^{2+}. This buffering is fast and is assumed to be at equilibrium. This allows the use of the rapid buffering approximation (Wagner and Keizer, 1994), which provides a buffering factor,

$$\beta = \left(1.0 + \frac{[Mg^{2+}]_{total} K_{MgPi}}{([P_i]_m + K_{MgPi})^2} + \frac{[Ca^{2+}]_{total} K_{CaPi}}{([P_i]_m + K_{CaPi})^2}\right)^{-1}, \tag{11}$$

where $[Mg^{2+}]_{total}$ and $[Ca^{2+}]_{total}$ are the total Mg^{2+} and Ca^{2+} concentrations, and K_{MgPi} and K_{CaPi} are the calcium and magnesium dissociation constants from P_i. The values measured by Corkey and co-workers (1986) were used. This buffering factor can be used in the dynamic

equations for $[P_i]_m$

$$\frac{d[P_i]_m}{dt} = \beta\left(-\frac{I_{mCS}}{zFW} - \frac{I_{ATP}}{3FW} + J_{pic} - \frac{I_{IMAC}}{zFW}\right), \quad (12)$$

where W is the mitochondrial matrix volume obtained as the product of the mitochondrial volume [25.2 pl obtained from Bers (2001)] and the (matrix volume):(mitochondrial volume) ratio [0.98 obtained from (Scalettar et al., 1991)]. The parameter F denotes Faraday's constant and z is the assumed average charge of P_i. The number three in the denominator of the term containing I_{ATP} represents the stoichiometry of three protons move into the mitochondria through the F_1F_0-ATPase to produce one ATP from one ADP and one P_i (Fillingame, 1997).

The rapid buffering approximation also allows for the calculation of $[Mg^{2+}]_m$ without another differential equation

$$[Mg^{2+}]_m = \frac{[Mg^{2+}]_{total}}{1.0 + \frac{[P_i]_m}{K_{MgPi}} + \frac{[ATP]_m}{K_{MgATP}} + \frac{[ADP]_m}{K_{MgADP}} + \frac{[AMP]_m}{K_{MgAMP}} + \frac{[GTP]_m}{K_{MgGTP}}}, \quad (13)$$

where K_{MgPi}, K_{MgATP}, K_{MgADP}, K_{MgAMP}, and K_{MgGTP} are the Mg^{2+} dissociation constants for P_i, ATP, ADP, AMP, and GTP, respectively. $[ATP]_m$, $[ADP]_m$, $[AMP]_m$, and $[GTP]_m$ are the mitochondrial matrix free ATP, ADP, AMP, and GTP concentrations, respectively.

The ADP/ATP translocase description is based on bi-substrate Michaelis–Menten kinetics and the experiments of Barbour and Chan (1981). In these experiments, they measured intake rate by the translocase when only ADP or only ATP was present. The translocase currents were characterized by Michaelis–Menten kinetics with velocities and binding constants for each case reported. The reverse rates were estimated in the model to ensure thermodynamic consistency (zero flux at equal concentrations inside and outside the mitochondria). The uptake of ADP and ATP by the translocase is described by

$$J_{ADP/ATP} = \frac{v_{ADP/ATP}\left[e^{0.7\Psi F/RT}\frac{[ADP]_i[ATP]_m}{K_{ADP,it}K_{ATP,m}} - e^{-0.3\Psi F/RT}\frac{[ADP]_m[ATP]_i}{K_{ADP,m}K_{ATP,i}}\right]}{1 + \frac{[ADP]_i}{K_{ADP,i}} + \frac{[ATP]_m}{K_{ATP,m}} + \frac{[ADP]_i[ATP]_m}{K_{ADP,i}K_{ATP,m}} + \frac{[ADP]_m}{K_{ADP,m}} + \frac{[ATP]_i}{K_{ATP,i}} + \frac{[ADP]_m[ATP]_i}{K_{ADP,m}K_{ATP,i}}}, \quad (14)$$

where $V_{ADP/ATP}$ is the velocity for the translocase, $K_{ADP,i}$ and $K_{ATP,i}$ are the binding constants for extramitochoindrial ADP and ATP, respectively, $K_{ADP,m}$ and $K_{ATP,m}$ are the binding constants for mitochondrial ADP and ATP, respectively, $[ADP]_i$ and $[ATP]_i$ are the extramitochondrial free ADP and ATP concentrations, respectively, and $[ADP]_m$ and $[ATP]_m$ are the mitochondrial free ADP and ATP concentrations respectively. The current generated by the translocase is ($I_{ADP/ATP} = J_{ADP/ATP}\ F\ W$) where F is Faraday's constant and W is the matrix volume. With this representation, we would like to point out that when one molecule of ADP is transported into the mitochondria, there is one molecule ATP transported out of the mitochondria and vise versa through the formation of a two ternary complexes with a random order of addition. The charge difference between ATP and ADP accounts for the current. During normoxic conditions extramitochondrial ATP concentration is 0.5 mM and extramitochondrial ADP concentration is 0.014 mM. During the experiments of Vergun and colleagues where they measured metabolic oscillations, the extramitochondrial ADP and ATP concentrations were zero.

To complete the model for metabolic oscillations a description of oscillations in flavoprotein fluorescence is needed. The mitochondria are the source of most of the NADH autofluorescence in cardiac myocytes (Eng et al., 1989). The electron transport chain accounts for most of the conversion of NADH to NAD^+ in the mitochondria. The citric acid cycle produces NADH from NAD^+ and is stimulated by NAD^+ and inhibited by [NADH]. The production of NADH by substrate dehydrogenation in the tricarboxylic acid cycle has been described by

$$J_{DH} = k_{DH}\frac{1}{\left(1 + \frac{K_{mN}}{[NAD^+]_m/[NADH]_m}\right)^{p_{DH}}} \quad (15)$$

based on the description developed by Korzeniewski and Zoladz (2001) where k_{DH} is the maximal rate of NADH production, $[NADH]_m$ is the mitochondrial matrix NADH concentration, $[NAD^+]_m$ is the mitochondrial matrix NAD^+ concentration, K_{mN} is the $[NAD^+]_m/[NADH]_m$ ratio that gives half maximal NADH production and p_{DH} is a cooperativity factor.

The balance equations for the mitochondrial NADH and NAD^+ concentration, respectively, are

$$\frac{d[NADH]_m}{dt} = \frac{I_{resp}}{3FW} + J_{DH}, \quad (16)$$

$$\frac{d[NAD^+]_m}{dt} = -\frac{I_{resp}}{3FW} - J_{DH}, \quad (17)$$

where the three in the denominator indicates that $3H^+$ ions are transported by the proton pumps for each NADH consumed.

Finally, based on the above relations we can determine the dynamic equation for the mitochondrial membrane

potential (Ψ)

$$\frac{d\Psi}{dt} = -\frac{1}{C_m}\left(I_{mCS} + I_{IMAC} + I_{resp} + I_{ATP} + I_{ADP/ATP} + I_{uniport} + I_{NaCaX} + I_{other}\right), \quad (18)$$

where C_m is the mitochondrial membrane capacitance obtained from Bers (Bers, 2001) and the currents are described above. The convention $\Psi > 0$ is assumed, which is consistent with other models (Korzeniewski and Zoladz, 2001; Magnus and Keizer, 1998). The experimental papers, however, tend to use negative sign. The current I_{other} includes the sum of all other currents not explicitly modeled and is set to be 8.1 pA.

3. Numerical methods

The model is described by a system of equation, which involves five ordinary differential equations. The differential equations were solved using Euler method with a time step of $dt = 0.00005$ s. The computations were performed on a HP C3000 workstation or a 1.86 GHz Compaq nw8240 laptop running Windows XP and cygwin. Visualization of the results was performed using the graphing software xmgr (freeware) or PV-WAVE (Precision Visuals, Inc.). Final figures were generated using PV-WAVE, Microsoft Excel, and Adobe Illustrator.

4. Results

The model was used to simulate various experimental protocols and the corresponding experimental observations: (1) resting mitochondria under normoxic conditions, (2) metabolic oscillations under ischemic conditions, (3) block of metabolic oscillations by addition of benzodiazepines and (4) the concentration changes of various native compounds (ADP, ATP, H^+, Mg^{2+}). Under resting normoxic conditions the simulated mitochondrial variables Ψ, $[P_i]_m$, $[Mg^{2+}]_m$, $[NADH]_m$, and $[NAD^+]_m$ assume values consistent with experimentally reported values as indicated in Table 2 (column 2). Under simulated ischemia (described below), the variables oscillate in the ranges indicated in Table 2 (column 3). During ischemia, cardiac myocytes are deprived of both oxygen and substrate. Without oxygen, the electron transport chain slows, resulting in a decrease in Ψ (Berkich et al., 2003). Similar effect can be observed during experiments on isolated mitochondria in which the oscillations occur (Vergun et al., 2003). There is also a decrease in cytosolic ATP and an increase in ADP and P_i. During ischemia the mitochondrial NADH rises and the pH falls. These conditions are simulated in the model by decreasing E_{resp} from 258 to 190 mV, increasing $[P_i]_i$ from 2.78 to 8.34 mM, and decreasing extramitochondrial pH from 7.1 to 7.0 and mitochondrial matrix pH from 7.6 to 7.1, respectively. Furthermore, when the magnitude of I_{resp} decreases ($I_{resp} < 0$) $[NADH]_m$ increases (Eqs. (1) and (16)), indicating that during simulated ischemia $[NADH]_m$ increases. In the model, while the changes in pH and $[P_i]_i$ are not necessary to produce oscillations, they do modulate the oscillations. The oscillations pictured have a period of ~60 s. The oscillations are quite robust in that parameter variations

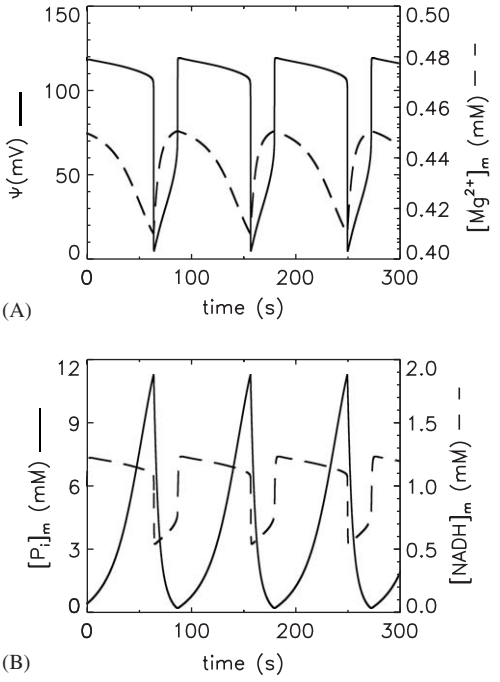

Fig. 2. Simulation of concentration changes during metabolic oscillations seen under ischemic conditions. (A) Mitochondrial membrane potential (solid line), mitochondrial magnesium concentration $[Mg^{2+}]_m$ (dashed line) and (B) Mitochondrial phosphate concentration ($[P_i]_m$; solid line), mitochondrial NADH concentration ($[NADH]_m$; dashed line).

Table 2
Variable values

Variable	Normoxic value	Ischemic values	Experimental value (Reference)
Ψ	160.2 mV	4.8–119.2 mV	150–180 mV (Skárka and Ostádal, 2002)
$[P_i]_m$	10.4 mM	0.23–11.3 mM	2.8–28.2 mM (Albe et al., 1990) 12.7 mM (Corkey et al., 1986)
$[Mg^{2+}]_m$	0.41 mM	0.41–0.45 mM	0.35–0.38 (Jung et al., 1997) 0.67 mM (Corkey et al., 1986)
$[NADH]_m$	0.96 mM	0.54–1.24 mM	$[NADH]_m$ = 1.1–2.3 mM (Livingston et al., 1996)
$[NAD^+]_m$	2.24 mM	1.96–2.66 mM	0.80–2.23 mM (Livingston et al., 1996)

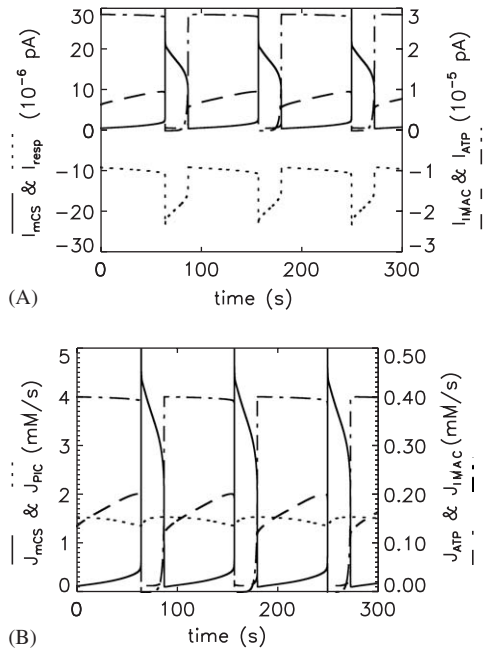

Fig. 3. Simulation of mitochondrial inner membrane currents and fluxes during metabolic oscillations seen under ischemic conditions. (A) mCS current (I_{mCS}; solid line); restorative current (I_{resi}; dotted line), IMAC current (I_{IMAC}; dashed line), ATP current (I_{ATP}; dash-dotted line) and (B) mPS flux (J_{mCS}; solid line); phosphate carrier flux (J_{PIC}; dotted line), IMAC flux (J_{IMAC}; dashed line), ATP flux (J_{ATP}; dash-dotted line).

can produce oscillations of different frequencies. During the oscillations pictured, the membrane potential Ψ (Fig. 2A; solid) ranges from 4.8 to 119.2 mV, the $[Mg^{2+}]_m$ (Fig. 2A; dashed) ranges from 0.41 to 0.45 mM, the $[P_i]_m$ (Fig. 2B; solid) ranges from 0.23 to 11.3 mM, and the $[NADH]_m$ (Fig 2B; dashed) ranges 0.54–1.24 mM. It is important to note that during membrane depolarization (and the decline in $[NADH]_m$), $[P_i]_m$ is high while $[Mg^{2+}]_m$ is low.

The oscillations are also accompanied by oscillations in the ionic currents across the inner mitochondrial membrane (Fig. 3A). The mCS current (I_{mCS}; Fig. 3A; solid) is the largest current causing the bulk of the depolarization. The membrane potential restorative current generated by the respiration-driven proton pumps (I_{resp}; Fig. 3A; dotted) opposes the depolarization and repolarizes Ψ. The IMAC low conductance channel (I_{IMAC}; Fig. 3A; dashed) causes a slow depolarization that brings Ψ to the threshold for activation of I_{mCS}. The F_1F_0-ATPase proton current (I_{ATP}; Fig. 3A; dash-dotted) shows transient decreases during Ψ depolarization.

Analysis of the behavior of these currents can give some insight into the mechanism of the metabolic oscillations, which will be discussed below. It is interesting to note that during the depolarization of Ψ, the respiration-driven proton pumps (I_{resp}) current increases. This means that NADH consumption occurs at a faster rate when the mitochondrial membrane potential is diminished as predicted by Murphy and Brand (1988a, b) in their experimental studies. The rationale behind this prediction is that at lower Ψ, the pumping of H^+ ions out of the mitochondria will be thermodynamically less expensive that at higher Ψ.

The major fluxes that govern $[P_i]_m$ are shown in Fig. 3B. The mCS channel current (Fig. 3B; solid) is the main source of P_i efflux during the depolarization of Ψ that occurs during the oscillations. With depolarization of Ψ the activity of the F_1F_0-ATPase decreases drastically (Fig. 3B; dash-dotted). These cyclic variations of ATP production can give rise to oscillations in ATP and ADP concentration that would result in oscillations of sarcolemmal $I_{K,ATP}$ and lead to the variation of action potential duration seen by O'Rourke and co-workers (1994). The activity of the phosphate carrier (PIC) also varies with the oscillations (Fig. 3B; dotted). When $[P_i]_m$ falls during the depolarization of Ψ, PIC activity increases replenishing $[P_i]_m$. Between depolarizations, mitochondrial P_i falls due to slow leakage of of P_i out of the mitochondria through the IMAC-LCC channel (Fig. 3B; dashed).

The mechanism for this can be described as follows: The initial decline in E_{resp} reduces Ψ so that the mCS channel, a voltage-dependent channel, is closer to its threshold for opening. The increase of $[P_i]_i$ is also crucial because the increased influx of P_i via the PIC leads to an increase in $[P_i]_m$ (Fig. 2B; solid). The increased P_i binds Mg^{2+}, which decreases $[Mg^{2+}]_m$ (Fig. 2B; dashed) increasing the open probability of IMAC–LCC which can be seen by increasing I_{IMAC} (Fig. 3A; dashed). Opening of IMAC–LCC results in depolarization of Ψ (Fig. 2A; solid), which results in opening of mCS (Fig. 3A; solid). The positive feedback of the opening of mCS yields a large current which rapidly depolarizes Ψ (Fig 2A; solid). Opening of mCS results in P_i efflux through the channel and a drop in $[P_i]_m$ (Fig. 2B; solid). This continues until $[P_i]_m$ falls sufficiently so that the mCS current diminishes. Activity of the PIC replenishes $[P_i]_m$ (Fig. 3B; dotted) and repolarizes Ψ resulting in a decrease in mCS open probability. The cycle then repeats.

PK11195 has also been shown to block mCS channel and IMAC with high affinity ($IC_{50} = 80$ nM) in mitoplasts (Kinnally et al., 1993). In experiments with isolated mitochondria and intact myocytes a significantly higher concentration (>100 μM) must be added to the bath in order to abolish oscillations. This can be attributed to decreased accessibility of the channel in intact cells when compared to the channel in mitoplast under patch clamp conditions (O'Rourke, 2000). In simulations, where the mCS conductance is reduced to 50% normal, i.e. 50% block (Fig. 4; between 100 and 200 s as indicated by the horizontal bar) or more the oscillations cease. When the block is removed at 200 s, the oscillations resume. During the period of block, the $[P_i]_m$ levels rise (Fig. 4B; dashed) while the $[Mg^{2+}]_m$ levels fall (Fig. 4A; dashed), both reaching a steady state value. The $[P_i]_m$ levels depend heavily on the properties of the phosphate carrier. To verify the essential role of the mCS channel use of a

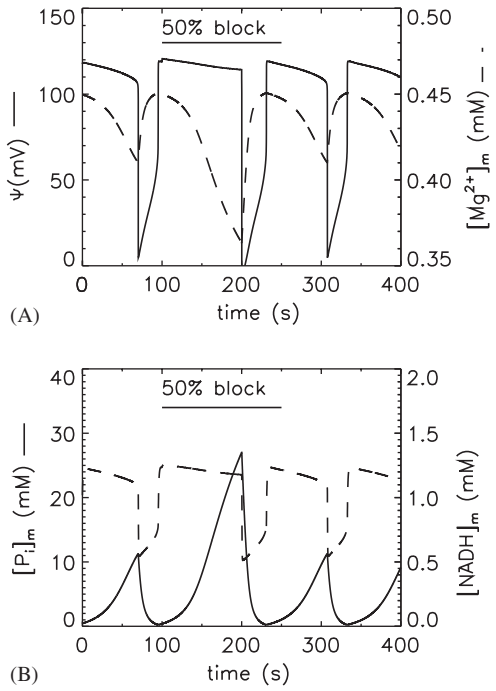

Fig. 4. Block of mCS reversibly terminates oscillations. The mCS current is reduced by 50% from 100 to 200 s during the simulation. (A) Oscillations in Ψ (solid line); $[Mg^{2+}]_m$ decreases during block (dashed line) and (B) $[P_i]_m$ rises during block (dashed line); $[NADH]_m$ oscillations cease during block (solid line).

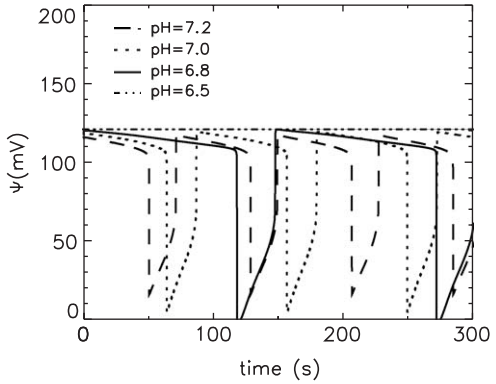

Fig. 5. Simulated metabolic oscillations show dependence on pH (pH = 7.2 ; dashed line), (pH = 7.0; dotted line), (pH = 6.8; solid line). A further drop in pH (pH = 6.5; dot-dashed line) abolishes the oscillations.

compound such as clonazepam that blocks mCS ($IC_{50} = 15\,\mu M$) but not IMAC–LCC should be tested (Kinnally et al., 1993). Block of IMAC (85% block) also reversibly terminates oscillations, consistent with the experimental finding that PK11195 addition reversibly terminates the metabolic oscillations (not shown).

Simulations with different pH values show that oscillations can be observed only in a certain pH range. This result is in line with experimental evidence (Chance and Yoshioka, 1966) showing that the pH has to be within optimal range for the oscillations to occur. The model predicts that decreasing the extramitochondrial pH from 7.2 (Fig. 5; dashed) to 7.0 (Fig. 5; dotted) to 6.8 (Fig. 5; solid) decreases the oscillation frequency. Further reduction of the pH to 6.5 terminates the oscillations (Fig. 5; dash-dotted). The mitochondrial pH is changed so that it remains 0.5 pH unit below the extramitochondrial pH (i.e. if extramitochondrial pH is changed to 7.2, the mitochondrial matrix pH is changed to 7.7).

The model suggests that changes in the cellular Mg^{2+} concentration would result in changes in the frequency of the metabolic oscillations. For example, double $[Mg^{2+}]_{total}$ results in an increase in the frequency and amplitude of the oscillations through its influence on IMAC–LCC open probability (not shown) over control. A five-fold increase in $[Mg^{2+}]_m$ abolishes the oscillations consistent with the observation by Bernardini and co-workers (1982) in liver mitochondria that agents that increase free Mg^{2+} from the membrane abolish oscillations.

Experiments have shown that addition of high concentration (100 μM) of ATP or ADP to isolated mitochondria kept in ADP and ATP free media reversibly inhibits the oscillations (Vergun et al., 2004). To simulate the experiments of Vergun and colleagues (2004), the extramitochondrial ATP, $[ATP]_e$ is increased to 100 μM from 100 to 200 s as shown in Fig. 6A by the bar. During this period the oscillations terminate. In this case the translocase provides a negative current as shown in Fig. 6C (long dashes). The case where there is not extramitochondrial ATP or ADP is show also with no current (short dashes). When the extramitochondrial ADP, $[ADP]_i$ is increased to 100 μM from 100 to 200 s as shown in Fig. 6B, the oscillations also terminate. Accompanying the addition of extramitochondrial ADP or ATP is a change in the current generated by the ADP/ATP translocase (Fig. 6C). When AMP or GTP are added external to the mitochondrial oscillations were not affected (Vergun et al., 2004). This is due to the fact that the translocase does not transport AMP or GTP although it does bind them (Pfaff and Klingenberg, 1968; Goto et al., 2002). This results in no change to the membrane currents and does not lead to oscillation termination. Hence the input of additional currents can move the model out of the oscillatory regime.

Import of ATP or ADP into the mitochondria is accompanied by extrusion of its counterpart. For example, ATP uptake is accompanied by ATP extrusion. This results in a no net change in nucleotide concentration. Given that the nucleotides bind Mg, we wanted to explore the magnitude of changes to the matrix ATP or ADP concentrations necessary to terminate oscillations. In the model, a step increase of 15.0 mM in ATP ($[ATP]_m$) is implemented (from 100 to 200 s as indicated by the horizontal bar), the oscillations cease during this time (Fig. 6D). A similar response is obtained by a step increase of 250.0 mM ADP in the model (not shown). Smaller concentrations do no reliable terminate the oscillations. In the simulations, addition of high concentrations of GTP or AMP, unlike ATP and ADP, do not terminate oscillations.

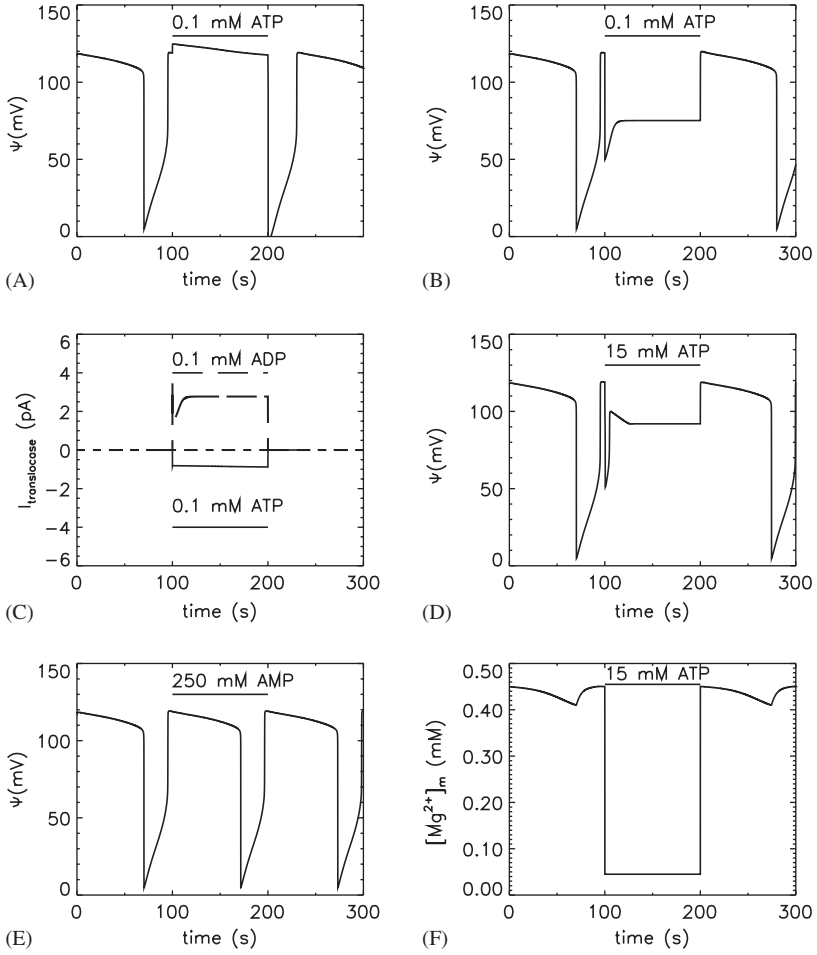

Fig. 6. Sensitivity of the simulated oscillations to adenine nucleotides. (A) Increased ATP concentration to 0.1 mM terminates the oscillations (from 100 s) in mitochondrial membrane potential (solid line); (B) increased ADP concentration to 0.1 mM terminates the oscillations (from 100 s); (C) increasing extramitochondrial ATP alone (solid bar) increases the ATP uptake current (solid trace). Increasing the extramitochondrial ADP alone (long dashed bar) increases the ADP uptake current (long dashed trace). If extramitochondrial ATP and ADP are zero, there is zero current (short dashed trace); (D) increase mitochondrial matrix ATP to 15 mM terminates oscillations; (E) increasing mitochondrial matrix AMP concentration to 250 mM does not terminate the oscillations; and (F) with the increased ATP concentration in D, the free matrix magnesium falls.

The model mimics this behavior for both AMP (Fig. 6E) and GTP (not shown) added at 100 s as indicated by the horizontal bar.

The mechanism behind this observation and simulation is demonstrated for ATP in Fig. 6F. In the model, ADP and ATP bind mitochondrial Mg^{2+} and hence serve as Mg^{2+} buffers. When a large amount of ATP or ADP is added, it results in a decreases in the $[Mg^{2+}]_m$ (Fig. 6F) which results in activation of IMAC–LCC. The increase in IMAC–LCC current moves the system out of the oscillatory regime. AMP and GTP do not abolish the oscillations because they do not significantly bind Mg^{2+} due to their lower affinity to Mg^{2+} compared to ATP and ADP. Hence, AMP and GTP exert little influence on IMAC–LCC.

Experiments have shown that blocking the electron transport chain at different points terminate the oscillations (Aon et al., 2003). In the model, reduction of the electron transport chain current (I_{resp}) terminates the oscillations. This can be accomplished by reducing E_{resp} from 190 to 150 mV or by reducing the whole current by increasing R_{resp}. In terms of the model, the reduction of I_{resp} reduces the restorative force for the membrane potential. Hence, during the depolarizing cycle of the oscillations, there is not sufficient current to repolarize the mitochondria.

Experiments performed by Vergun and co-workers (2004) demonstrated how cytosolic Ca^{2+} influences the oscillations. Application of ruthenium red, a blocker of the Ca^{2+} uniporter, terminated the oscillations. The uniporter uses Ψ as a driving force to move Ca^{2+} into the mitochondria. It provides a depolarizing current. The model simulates this behavior in Fig. 7A where application of ruthenium red (simulated by setting P_{Ca} to zero) at 100 s terminates the oscillations. Similar to the experiments accompanying the block, there is a rise in Ψ to a plateau value. Vergun and colleagues also added 100.0 μM EGTA, a chelator of calcium, outside the mitochondria and

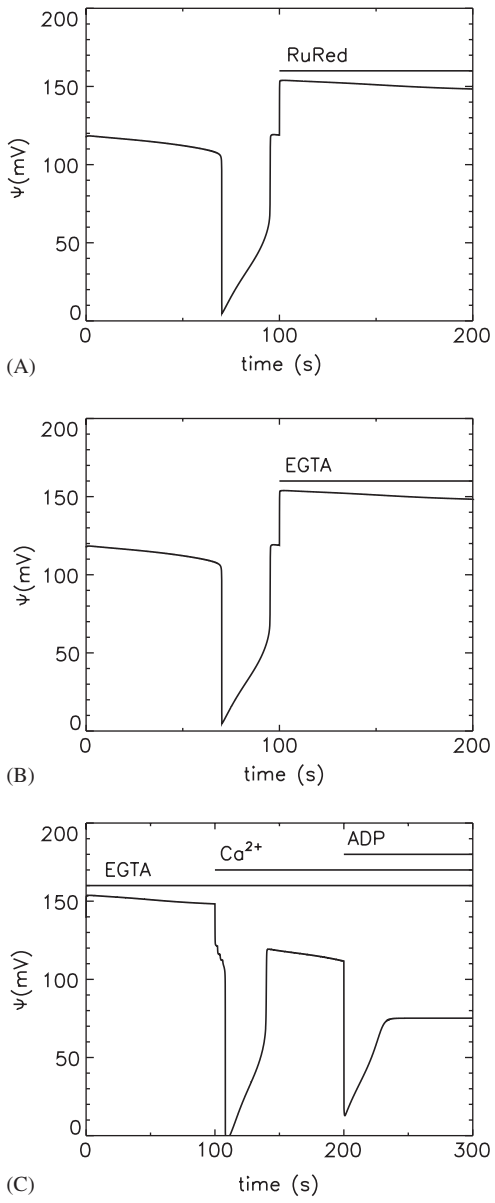

Fig. 7. The effects of mitochondrial calcium dynamics on metabolic oscillations. (A) Blocking Ca uniporter at 100 s by adding ruthenium red (RuRed) terminates the oscillations and increases membrane potential; (B) buffering Ca^{2+} by 100 EGTA at 100 s terminates the oscillations and increases membrane potential; and (C) combination of 100 EGTA and 100 Ca from 100 to 200 s elicits oscillations. Adding 100 μM ADP at 200 s in addition to EGTA and Ca terminates the oscillations.

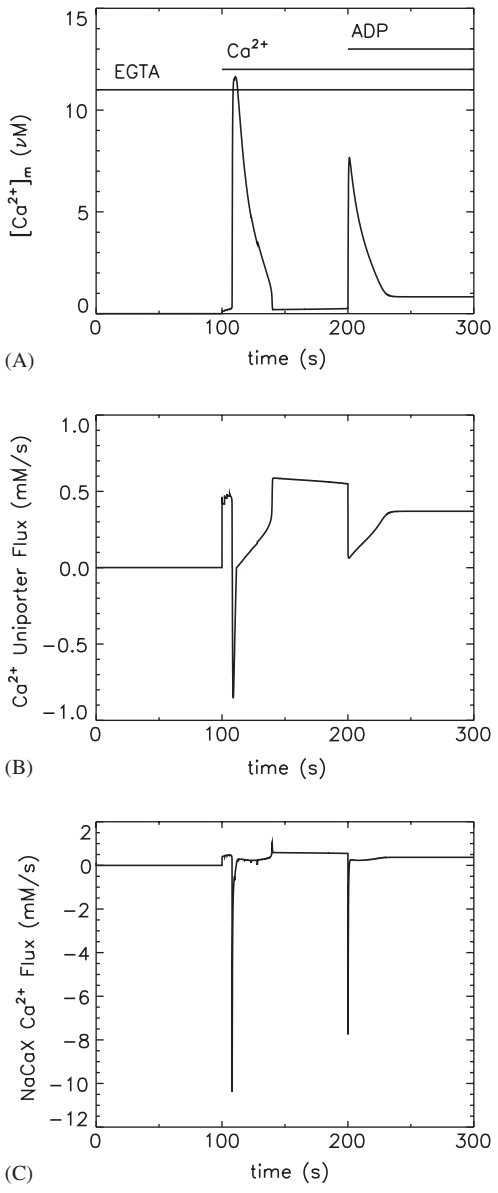

Fig. 8. Changes to calcium uptake and extrusion during simulated experimental protocols. EGTA binds all mitochondrial calcium (under 100 s). Increasing cytosolic Ca^{2+} concentration elicits oscillations in mitochondrial Ca^{2+} (from 100 to 200 s). Adding ADP together with EGTA at increased cytosolic Ca^{2+} levels terminates the oscillations in mitochondrial Ca^{2+} although free mitochondrial calcium is present (above 200 s). A. Similar pattern is observed for uniporter flux and B. Na^+/Ca^{2+} exchanger flux.

terminated the oscillations. An additional equation using the rapid buffering approximation to describe Ca^{2+} binding by EGTA was added to the model ($[Ca^{2+}]_{free} = [Ca^{2+}]/(1 + [EGTA/]/K_{Ca,EGTA})$). When 100.0 μM EGTA is added at 100.0 s oscillations terminate with Ψ rising to a plateau value similar to experiment (Fig. 7B). Vergun and co-workers also performed a more complex experimental protocol in which they added EGTA external to the mitochondria terminating the oscillations. Upon addition of Ca^{2+} the oscillations resumed. When ADP was added in addition to the already present EGTA and Ca^{2+}, the oscillations terminate. The model simulates this behavior well as shown in Fig. 7C. In the presence of 100.0 μM EGTA there are no oscillations. When 100.0 μM Ca^{2+} is added at 100 s, oscillations resume. When 0.1 mM ADP is added at 200 s, the oscillations terminate in a plateau lower than the plateau seen with EGTA alone similar to the experiments.

The model can demonstrate the mechanism responsible for this behavior. Fig. 8A shows that in the presence of EGTA, $[Ca^{2+}]_m$ is low as is $[Ca^{2+}]_i$ (not shown). The low value of $[Ca^{2+}]_m$ is due to little influx of calcium through

the uniporter as indicated in Fig. 8B by the near zero uniporter current during the first 100 s. Accompanying the low $[Ca^{2+}]_m$ is a near zero mitochondrial Na^+–Ca^{2+} exchanger flux, since there is little calcium to clear (Fig. 8C). When 100 μM Ca^{2+} is added externally, it overcomes the buffering of EGTA returning $[Ca^{2+}]$ to normal levels (0.1–0.2 μM) from 100–120 s (Fig. 8A) by a resumption of uniporter flux (Fig. 8B). Along with the restoration of $[Ca^{2+}]_m$ is a resumption of Ca^{2+} extrusion by the Na^+–Ca^{2+} exchanger (Fig. 8C). With the resumption of the uniporter and exchanger currents oscillations can resume. Simulations where these currents changes influence the membrane potential without altering calcium dynamics terminate the oscillations. The influence of ADP occurs without altering Ca^{2+} dynamics but through its effect on free $[Mg^{2+}]_m$ as shown in Fig. 6.

5. Discussion

The oscillations produced by the model display behavior characteristic of Hopf bifurcations. More specifically, as certain bifurcation parameters, such as G_{IMAC}, E_{resp}, or [ADP], are varied, the system moves from steady-state behavior to oscillatory behavior and back to steady-state behavior. Under the parameters studies performed no period doubling behavior were observed.

Each mitochondrion consists of the mitochondrial membrane, the intramembrane space, and the mitochondrial matrix. In the model, the mitochondrial matrix is assumed to be a single, well-mixed (homogeneous) compartment. This is a commonly used assumption to make modeling more tractable. While there might be spatial heterogeneity in the matrix, the measurements taken in many experiments are averaged over space and do not resolve matrix heterogeneity.

In Fig. 6, additions of 0.1 mM ATP or ADP terminate the oscillations through a change in the ADP/ATP translocase current. In the case of ATP additions this is a negative current. On the other hand, addition of ADP results in a positive current. These concentrations are in agreement with the experimental finding of Vergun and colleagues (2004). Compounds such as AMP and GTP do not cause a current as they are not transported by the translocase. The model also tests what magnitude change to mitochondrial ATP or ADP concentrations would be needed to terminate oscillations due to their effect on free mitochondrial Mg^{2+}. Addition of 15 mM of ATP or addition of 250 mM of ADP were required to abolish oscillations. These values are both greater than the experimental amount used by Vergun and co-workers (2004). This suggests that it is the contribution of current rather than changes in free mitochondrial Mg^{2+} that terminate the oscillations. In the model, ADP, ATP, GTP, and AMP addition is made directly to the mitochondrial matrix.

The model finding that a mitochondrial ADP concentration 15-fold higher than the ATP concentration is needed to terminate oscillations can be explained in terms of the ATP and ADP binding affinities for Mg^{2+}. ATP binds Mg^{2+} with 16.6 times higher affinity than does ADP. This means that 250 mM ADP binds approximately as much Mg^{2+} as does 15 mM ATP. The experimental findings use a similar concentration of ATP or ADP external to the mitochondrial to terminate oscillations. Under normoxic conditions the ADP/ATP translocase displays a higher affinity for ADP than ADP (100–120 μM vs. 2–4 μM, respectively). However, in uncoupled mitochondria, the affinity for ATP increases to 6–10 μM and the affinity for ADP decreases to 30–35 μM (Barbour and Chan, 1981). Hence the addition of external ADP or ADP will enter the ischemic mitochondria more easily than would ATP.

This model proposes a mechanism for metabolic oscillations. The model makes a number of assumptions to simplify the complexity of the phenomenon: (1) The binding of Mg^{2+} and P_i is fast so the reaction is assumed to be in equilibrium; (2) The binding of Ca^{2+} and P_i is fast and in equilibrium; (3) The binding of Mg^{2+} to ATP and ADP is fast and in equilibrium; (4) the pH, [ADP], and [ATP] of mitochondrial matrix remain constant over the course of an oscillation; (5) The only charge carrier is P_i through the anion channels and it assumes an average valence of −2. The assumption of rapid equilibrium reduces the number of differential equations. Including the dynamics of binding would not appreciably alter the behavior of the model. It is also important to note that while the association of calcium and phosphate might be rapid, the precipitation of calcium phosphate is a slower process that occurs at high matrix calcium. The assumption that pH remains constant is made for simplicity. It is indeed likely as indicated by the experiments of Bernardi and colleagues (1982) that the proton concentration might oscillate during metabolic oscillations. Oscilations in pH would likely modulate the oscillations through their effect on the IMAC–LCC channel. In order to capture this behavior correctly the details of proton balance would have to be included. No mitochondrial model to date models proton balance in the mitochondria. The assumption that the mitochondrial ATP and ADP concentrations remain relatively constant is based on the assumption that the adenine nucleotide translocase is rapid. If fluctuations in ADP and ATP did occur, they might affect the F_1F_0-ATPase activity as well as the ATP-sensitive potassium channel which would modulate the oscillations through their effect on membrane potential. Finally the assumption that P_i is the only charge carrier through the ion channels was made so the model would only have to have balance equations for one ion. In fact other anions such as Cl^- also flow through the channel. These other anions would likely result in more depolarization and less change in phosphate concentration during the oscillations.

The model uses a simplified model of the F_1F_0-ATPase that is based on the voltage dependence observed by Kaim and Dimroth in *Escherinchia coli* and *Propionigenium modestum*. A similar relation was observed by Berkich

and co-workers (1991) in cardiac myocyte mitochondria. The model does not include the pH gradient as this is not the major regulatory factor. The ATP and ADP concentration dependence of the ATPase as these are constant in the model ($[ATP]_{mito} = 0.44\,mM$ and $[ADP]_{mito} = 2.49\,mM$). Furthermore, the binding constants used by Westerhoff and co-workers (1995) to describe the ADP/ATP dependence of the ATPase are $K_{ADP} = 0.0015\,mM$ and $K_{ATP} = 0.15\,mM$. Therefore, at these concentrations there is little possibility of reversal of the F_1F_0-ATPase. To be certain that the reaction is thermodynamically consistent. The free energy can be calculated for the different conditions of the model using the following equations for the free energy from the membrane potential and for the chemical reaction (Bromberg, 1984):

$$\Delta G^{pmf} = zFV + RT\ln\left(\frac{[H]_i}{[H]_m}\right),$$

$$\Delta G^{chem} = \Delta G^0 + RT\ln\left(\frac{[ADP][P_i]}{[ATP]}\right).$$

These are positive if ATP production is favorable and negative if ATP breakdown is favorable. In the steady state and throughout the conditions of the oscillations the free energy remains favorable for ATP production by the ATPase. With the conditions in the model $\Delta G^{chem} = 2385\,J/mol$ and $\Delta G^{pmf} = 16034\,J/mol$.

The model makes some assumptions as it does not explicitly describe the dynamics of mitochondrial matrix ADP concentration ($[ADP]_m$), mitochondrial matrix ATP concentration ($[ATP]_m$), or mitochondrial matrix proton concentration ($[H]_m$). While these undoubtedly change during metabolic oscillations and serve to modulate the oscillations, it is important to test that they do so in balance at steady-state conditions. The balance of $[ADP]_m$ is determined by the F_1F_0-ATPase and ADP/ATP translocase. Their steady-state currents are $I_{ATP} = 9.6 \times 10^{-7}\,\mu A$ and $I_{ADP/ATP} = 9.6 \times 10^{-7}\,\mu A$ being nearly balanced with a small difference of $7.0 \times 10^{-9}\,\mu A$. The proton balance is determined by I_{resp} ($-1.2 \times 10^{-5}\,\mu A$), $I_{ATP} = (2.9 \times 10^{-6}\,\mu A)$, I_{PIC} ($1.9 \times 10^{-6}\,\mu A$), Na^+/H^+ exchange which should stoichiometrically balance the Na^+/Ca^{2+} exchange ($5.6 \times 10^{-6}\,\mu A$) and the other currents ($I_{other} = 8.1 \times 10^{-7}\,\mu A$). This yields a difference which can be accounted for by electroneutral K^+/H^+ exchange ($-9.4 \times 10^{-7}\,\mu A$). In future work the details of nucleotide balance and proton balance can be incorporated into the model.

The model suggests that changes in pH might lead to changes or even termination of the metabolic oscillations. The effects of pH on the metabolic oscillation frequency only reflect its effect on the IMAC–MCC channel. Changes to mitochondrial pH might have additional effects on other aspects that might affect the oscillations, such as mitochondrial calcium handling. Experiments show that decreases in mitochondrial pH are accompanied by mitochondrial depolarization and a decrease in calcium uptake (Gursahani and Schaefer, 2004). It is likely that the reduced membrane potential decreases uptake by the uniporter (Kirichok et al., 2004). There have also been reports that decreases in pH also can decrease Na^+-dependent Ca^{2+} efflux (Na^+/Ca^{2+} exchange) from the mitochondria as well as respiration dependent calcium uptake (uniporter) into the mitochondria (Fry and McGuigan, 1990). While these effects are opposite, the mitochondrial calcium concentration might change. The changes, depending on their magnitude, can possibly lead to changes or termination of the oscillations as demonstrated in Fig. 9.

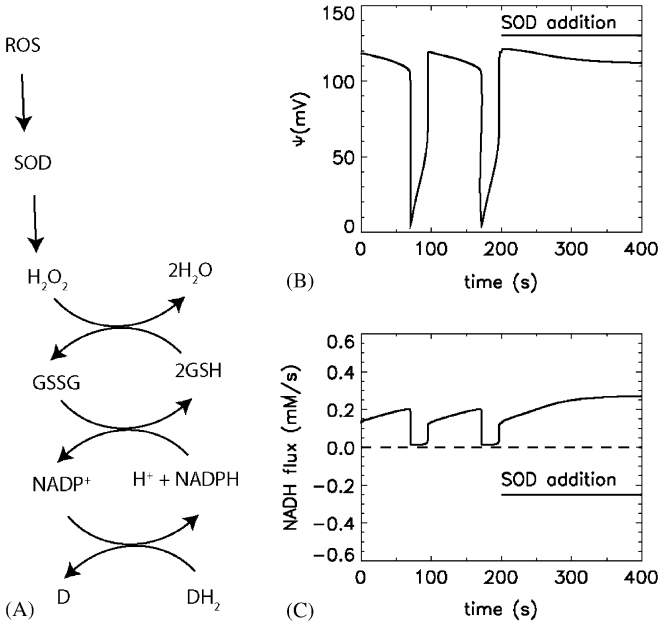

Fig. 9. The mechanism by which superoxide dismutase (SOD) might terminate oscillations. (A) ROS are converted to hydrogen peroxide (H_2O_2) which is degraded by catalase which converts reduced glutathione (GSH) to oxidized glutathione (GSSG). The GSSG is reduced by the conversion of NADPH to $NADP^+$. Then NADPH is reduced by passing some other reducing system; (B) Addition of SOD simulated as a 0.1 mM NADH generating flux to the mitochondria at 100 s terminates the oscillations; and (C) The NADH consumption flux (solid line) and the SOD related flux (dashed line).

In spite of the simplicity of the model, it produces a wide array of experimentally observed phenomena. The model produces metabolic oscillations under simulated ischemia. It shows that the oscillations only occur in a range of pH values and not outside this range as observed in experiments (Chance and Yoshioka, 1966). It correctly simulated that high levels of Mg^{2+} abolish the oscillations as observed by Bernardini and co-workers (1982). The model presents a mechanism that is sensitive to the ATP, ADP, AMP, and calcium similar to the experimental observations of Vergun and colleagues (2003, 2004). The model also presents a mechanism independent of the PTP consistent with experiments (Cortassa et al., 2004; Vergun et al., 2003).

Another hypothesis for metabolic oscillations that involves ROS has been proposed (Cortassa et al., 2004).

This model relies on a ROS-dependent opening of the IMAC channel. While they attribute this to work by Beavis (1992), this cited work indicates that the IMAC–LCC channel is sensitive to protons and does not indicate that it is redox sensitive. Furthermore, ROS is known to open the PTP which is a voltage-dependent channel in the mitochondrial inner membrane, activated by matrix Ca^{2+} and inhibited by matrix H^+.

The most direct method to test the involvement of PTP in cellular processes is based on calcein distribution (Petronilli et al., 1998). Based on these facts the increased levels of ROS in the phenomenon of metabolic oscillations should result in PTP opening and, subsequently, calcein redistribution from the matrix to the cytoplasm. However, the authors of the ROS-based hypothesis experimentally proved no calcein redistribution (Aon et al., 2003) and concluded that no PTP opening could be observed. This observation is consistent with the results from another group (Vergun et al., 2003) who also denied PTP opening. Their experiments showed also that ROS scavengers do not effect on the oscillations. Based on this data it seems unlikely that ROS levels are significantly increased since it would result in PTP opening.

Another impediment in the ROS-based model comes from the assumption on IMAC permeability to free radicals, which has not been proved yet. Finally, in order for this hypothesis to be correct, free radicals should be abundant on the matrix side of the mitochondrial inner membrane. It has been shown, however, that ROS production comes mostly from complex III of the mitochondrial electron transport chain (Chen et al., 2003), which releases superoxide on the cytoplasmic side of the mitochondrion (St-Pierre et al., 2002).

There is no question that there are ROS oscillations in conjunction with the metabolic oscillations (Cortassa et al., 2004). As the mitochondrial membrane potential changes, ROS production from the complex I and III of the electron transport change will vary. Aon and co-workers (2003) have observed that addition of superoxide dismutase (SOD) a ROS scavenger to the oscillating mitochondrial abolishes the oscillations. They assume that this is due to removal of ROS. To understand this phenomenon better, it is important to understand how SOD removes ROS (DeRobertis & DeRobertis Jr., 1987). SOD removes the oxygen radical and creates hydrogen peroxide (Fig. 9A). In the mitochondria catalase degrades the hydrogen peroxide by oxidizing glutathione. Glutathione is then reduced by oxidizing NADPH. This is reduced by a NADP-reducing system which could involve the generation of NADH. This newly produced NADH can enter the electron transport chain, augmenting the respiration-driven proton pumps which will terminate oscillations. Simulations of the addition of SOD with the model presented in this paper show that when NADH is increased by less than 3%, oscillations terminate (Fig. 9A,C). As a result, this model can explain the experimental observation that addition of SOD can terminate oscillations (Aon et al., 2003).

6. Conclusions

A computational model for the mechanisms producing metabolic oscillations in ischemic cardiac myocytes has been proposed. The model includes the low-conductance mitochondrial IMAC, the mCS, the mitochondrial phosphate carrier (PIC), the F_1F_0-ATPase, respiration-driven proton pumps, and the interactions of mitochondrial matrix P_i and Mg^{2+} with each other and with their buffers. The parameters of the model are determined by the physiological measurements from the experimental literature and yield current fluxes consistent with experimentally measured or estimated values. The model accounts for the oscillations in mitochondrial membrane potential, ATP-production and NADH levels observed experimentally.

The model suggests that while block of the IMAC reversibly abolishes the metabolic oscillations, IMAC alone is not enough to cause the oscillations due to the lack of strong enough positive feedback. The model suggests that the voltage-dependent mCS channel is a possible source of such feedback. The IMAC does play a crucial role as it slowly depolarizes Ψ until it reaches a threshold for mCS opening. A decrease of the inner membrane potential due to ischemia or experimental conditions seems to be an essential factor for the oscillations.

The model includes a subset of the ionic mechanisms contained in the mitochondria and hence does not show the full range of behaviors of the mitochondria. It does, however, suggest the minimal components necessary to produce sustained metabolic oscillation. The model has been validated based on simulation of experimentally observed behavior produced by changes in the ionic concentrations for ATP, ADP, Mg^{2+}, and H^+ as well as changes in electron transport rate. Furthermore, the model suggests a plausible mechanism for metabolic oscillations and predicts additional behaviors not reported in the experimental literature. Inclusion of the model such as this into whole ventricular myocyte network models would provide a medium to explore the effect of metabolic oscillations on cardiac arrhythmia formation.

Acknowledgements

This work was supported in part by National Academy of Sciences grant for Collaboration in Basic Science and Engineering. Partial support came from a Biomedical Engineering Research Grant from the Whitaker Foundation while M. S. Jafri and M. Kotulska were at the University of Texas at Dallas in the Department of Mathematical Sciences. Part of this work was performed while M. S. Jafri was an Adjunct Investigator at the Laboratory of Cardiac Energetics of the National Heart Lung and Blood Institute of the NIH. The authors would like to thank Patrick Gillevet for his helpful comments on the manuscript.

References

Albe, K.R., Butler, M.H., Wright, B.E., 1990. Cellular concentrations of enzymes and their substrates. J. Theor. Biol. 143 (2), 163–195.

Aon, M.A., Cortassa, S., Marban, E., O'Rourke, B., 2003. Sychronized whole cell oscillations in mitochondrial metabolism triggered by a local release of reactive oxygen species in cardiac myocytes. J. Biol. Chem. 278 (45), 44735–44744.

Armiger, L., Headrick, J., Jordan, L., Willis, R., 1995. Bound inorganic phosphate and early contractile failure in global ischemia. Basic Res. Cardiol. 90, 482–488.

Barbour, R.L., Chan, S.H.P., 1981. Characterization of the kinetics and mechanism of the mitochondrial ADP–ATP carrier. J. Biol. Chem. 256 (4), 1940–1948.

Beavis, A., 1992. Properties of the inner membrane anion channel in intact mitochondria. J. Bioenerg. Biomembr. 24 (1), 77–90.

Beavis, A., Powers, M., 1989. On the regulation of the mitochondrial inner membrane anion channel by magnesium and protons. J. Biol. Chem. 264 (29), 17148–17155.

Berkich, D.A., Salama, G., LaNoue, K.F., 2003. Mitochondrial membrane potentials in ischemic hearts. Arch. Biochem. Biophys. 420, 279–286.

Berkich, D.A., Williams, G.D., Masiakos, P.T., Smith, M.B., D., B.P., LaNoue, K.F., 1991. Rates of various reactions catalyzed by ATP synthase as related to the mechanisms of ATP synthesis. J. Biol. Chem. 266, 123–129.

Bernardini, P., Pozzan, M., Azzone, G.F., 1982. Mitochondrial oscillations and activation of H^+/cation exchange. J. Bioenerg. Biomembr. 14 (5/6), 387–403.

Bers, D., 2001. Excitation-Contraction Coupling and Cardiac Contractile Force. Developments in Cardiovascular Medicine, Second ed. Kluwer Academic Publishers, Dordrecht, p. 237.

Brady, N.R., Elmore, S.P., van Beek, J.J.H.G.M., Krab, K., Courtoy, P.J., 2004. Coordinated behavior of mitochondria in both space and time: a reactive oxygen species-activated wave of mitochondrial depolarization. Biophys. J. 87, 2022–2034.

Bromberg, J.P., 1984. Physical Chemistry, Second ed. Allyn and Bacon, Inc., United States, pp. 341–347.

Chance, B., Yoshioka, T., 1966. Sustained oscillations of ionic constituents of mitochondria. Arch. Biochem. Biophys. 117 (2), 451–465.

Chen, Q., Vasquez, E.J., Moghaddas, S., Hoppel, C.L., Lesnefsky, E.J., 2003. Production of reactive oxygen species by mitochondria: central role of complex III. J. Biol. Chem. 278, 36027–36031.

Corkey, B., Duszynski, J., Rich, T., Matschinsky, B., Williamson, J., 1986. Regulation of free and bound magnesium in rat hepatocytes and isolated mitochondria. J. Biol. Chem. 261 (6), 2567–2574.

Cortassa, S., Aon, M.A., Marban, E., Winslow, R.L., O'Rourke, B., 2003. An integrated model of cardiac mitochondrial energy metabolism and calcium dynamics. Biophys J 84, 2734–2755.

Cortassa, S., Aon, M.A., Winslow, R.L., O'Rourke, B., 2004. A Mitochondrial Oscillator Dependent on Reactive Oxygen Species. Biophys. J. 87, 2060–2073.

DeRobertis, E., DeRobertis Jr., E., 1987. Cell and Molecular Biology, eighth ed. Lea and Febiger, Philadelphia.

DiLisa, F., Blank, P., Gambassi, G., Silverman, H., Stern, M., Hansford, R., 1995. Mitochondrial membrane potential in single living adult rat cardiac myocytes exposed to anoxia or metabolic inhibition. J. Physiol. 486, 1–13.

Donoso, P., Mill, J.G., O'Neill, S.C., Eisner, D.A., 1992. Fluorescent measurements of cytoplasmic and mitochondrial sodium concentrations in rat ventricular myocytes. J. Physiol. 448, 493–509.

Eng, J., Lynch, R.M., Balaban, R.S., 1989. Nicotinamide adenine dinucleotide fluorescence spectroscopy and imaging of isolated cardiac myocytes. Biophys. J. 55, 621–630.

Fillingame, R.H., 1997. Coupling H^+ transport and ATP synthesis in F_1F_0-ATPase synthases: glimpses of interacting parts in a dynamic molecular machine. J. Exp. Biol. 200, 217–224.

Frenkel, R., 1968. Control of reduced diphosphopyridine nucleotide oscillations in beef heart extracts. II. Oscillations of glycolytic intermediates and adenine nucleotides. Arch. Biochem. Biophys 125 (1), 157–165.

Fry, C.H., McGuigan, J.A., 1990. The influence on pH and Ca^{2+} exchange in ferret heart mitochondria. Biochem. Biophys. Res. Comm. 166 (3), 1352–1357.

Ghosh, A., Chance, B., 1964. Oscillations of glycolytic intermediates in yeast cells. Biochem. Biophys. Res. Comm. 16 (2), 174–181.

Gooch, V., Packer, L., 1971. Adenine nucleotide control of heart mitochondrial oscillations. Biochim. Biophys. Acta 245 (1), 17–20.

Gooch, V., Packer, L., 1974. Oscillatory states of mitochondria. Studies on the oscillatory mechanism of liver and heart mitochondria. Arch. Biochem. Biophys. 163 (2), 759–768.

Goto, S., Chuman, H., Majima, E., Terada, H., 2002. How does the mitochondrial ADP/ATP carrier distinguish transportable ATP and ADP from untransportable AMP and GTP? Dynamics modeling of the recognition/translocation process in the major substrate binding region. Biochim Biophys. Acta. 1589 (2), 203–218.

Gursahani, H.I., Schaefer, S., 2004. Acidification reduces mitochondrial calcium uptake in rat cardiac mitochondria. Am. J. Physiol. Heart Circ. Physiol. 287, H2659–H2665.

Hagedorn, P.H., Flyvbjerg, H., Moller, I.M., 2004. Modeling NADH turnover in plant mitochondria. Physio Plantarum 120, 370–385.

Hochachka, P., 1999. The metabolic implications of intracellular circulation. Proc. Natl. Acad. Sci. USA 96 (22), 12233–12239.

Jung, D., Panzeter, E., Baysal, K., Brierley, G., 1997. On the relationship between matrix free Mg^{2+} concentration and total Mg^{2+} in heart mitochondria. Biochim. Biophys. Acta 1320 (3), 310–320.

Kaim, G., Dimroth, P., 1999. ATP synthesis by F-type ATP synthase is obligatorily dependent on the transmembrane voltage. EMBO J 18 (15), 4118–4127.

Kinnally, K., Antonenko, Y., Snyder, S., McEnery, M., Tedeschi, H., 1993. Mitochondrial benzodiazepine receptor linked to inner membrane ion channels by nanomolar actions of ligands. Proc. Natl. Acad. Sci. USA 90 (4), 1374–1378.

Kinnally, K., Antonenko, Y., Zorov, D., 1992. Modulation of Inner Mitochondrial Membrane Channel Activity. J. Bioenerg Biomembr. 24 (1), 99–110.

Kirichok, Y., Krapivinsky, G., Clapham, D.E., 2004. The mitochondrial calcium uniporter is a highly selective ion channel. Nature 427, 360–364.

Knox, B.E., Tsong, T.Y., 1984. Voltage-driven ATP synthesis by beef heart mitochondrial F1F0-ATPase. J. Biol. Chem. 259, 4757–4763.

Korzeniewski, B., Zoladz, J.A., 2001. A model of oxidative phosphorylation in mammalian skeletal muscle. Biophys. Chem. 92, 17–34.

Livingston, B., Altschuld, R., Hohl, C., 1996. Metabolic compartmentalization in neonatal swine myocytes. Pediatr. Res. 40 (1), 59–65.

Lloyd, D., Eshantha, L., Salgado, J., Turner, M., Murray, D., 2002. Respiratory oscillations in yeast: clock-driven mitochondrial cycles of energization. FEBS Lett 519 (1–3), 41–44.

Magnus, G., Keizer, J., 1997. Minimal Model of beta-cell mitochondrial Ca^{2+} handling. Am. J. Physiol. 273 (2, Part 1), C717–C733.

Magnus, G., Keizer, J., 1998. Model of beta-cell mitochondrial calcium handling and electrical activity. I. Cytoplasmic variables. Am. J. Physiol. 274 (4, Part 1), C1158–C1173.

Mironov, S., Richter, D., 2001. Oscillations and hypoxic changes of mitochondrial variables in neurons of the brainstem respiratory centre of mice. J. Physiol. 533 (Part 1), 227–236.

Murphy, M., Brand, M., 1988a. Membrane-potential-dependent changes in the stoichiometry of charge translocation by the mitochondrial electron transport chain. Eur. J. Biochem. 173 (3), 637–644.

Murphy, M., Brand, M., 1988b. The stoichiometry of charge translocation by cytochrome oxidase and the cytochrome bc1 complex of mitochondria at high membrane potential. Eur. J. Biochem. 173 (3), 645–651.

Murphy, R., Diwan, J., King, M., Kinnally, K., 1998. Two high conductance channels of the mitochondrial inner membrane are

independent of the human mitochondrial genome. FEBS Lett. 425 (2), 259–262.

Nyguen, M.-H.T., Jafri, M.S., 2005. Mitochondrial calcium signalling and energy metabolism. Ann. N. Y. Acad. Sci. 1047, 127–137.

O'Rourke, B., 2000. Pathophysiological and protective roles of mitochondrial ion channels. J. Physiol. 529 (1), 23–36.

O'Rourke, B., Ramza, B., Marban, E., 1994. Oscillations of membrane current and excitability driven by metabolic oscillations in heart cells. Science 265 (5174), 962–966.

Petronilli, V., Miotto, G., Canton, M., Colonna, R., Bernardi, P., DiLisa, F., 1998. Imaging the mitochondrial permeability transition pore in intact cells. Biofactors 8, 263–272.

Pfaff, E., Klingenberg, M., 1968. Adenine nucleotide translocation of mitochondria. I. Specificity and control. Eur. J. Biochem. 6, 66–79.

Romashko, D., Marban, E., O'Rourke, B., 1998. Subcellular metabolic transients and mitochondrial redox waves in heart cells. Proc Natl Acad Sci USA 95 (4), 1618–1623.

Sato, K., Kashiwaya, Y., Keon, C.A., Tsuchiya, N., King, M.T., Radda, G.K., Chance, B., Clarke, K., Veech, R.L., 1995. Insulin, ketone bodies, and mitochondrial energy transduction. FASEB J 9, 651–658.

Scalettar, B., Abney, J., Hackenbrock, C., 1991. Dynamics, structure, and function are coupled in the mitochondrial matrix. Proc Natl Acad Sci USA 88 (18), 8057–8061.

Skárka, L., Ostádal, B., 2002. Mitochondrial membrane potential in cardiac myocytes. Physiol. Rres. 51, 425–434.

Stappen, R., Krämer, R., 1994. Kinetic mechanism of phosphate/phosphate and phosphate/OH^- antiports catalyzed by reconstituted phosphate carrier from beef heart mitochondria. J. Biol. Chem. 269 (15), 11240–11246.

St-Pierre, J., Buckingham, J.A., Roebuck, S.J., Brand, M.D., 2002. Topology of superoxide production from different sites in the mitochondrial electron transport chain. J. Biol. Chem. 277, 44784–44790.

Taegtmeyer, H., King, L., Jones, B., 1998. Energy substrate metabolism, myocardial ischemia, and targets for pharmacotherapy. Am. J. Cardiol. 82 (5A), 54K–60K.

Trollinger, D.R., Cascio, W.E., Lemasters, J.J., 2000. Mitochondrial calcium transients in adult rabbit cardiac myocytes: inhibition by ruthenium red and artifacts caused by lysosomal loading of Ca^{2+}-indicating fluorophores. Biophys J. 79, 39–50.

Velden, J.V.D., Klein, L., Zaremba, R., Boontje, N., Huybregts, J., Stooker, W., Eigsman, L., Jong, J.D., Visser, C., Visser, F., Stienen, G., 2001. Effects of calcium, inorganic phosphate, and pH on Isometric force n single skinned cardiomyocytes from donor and failing human hearts. Circulation 104 (10), 1140–1146.

Vergun, O., Votyakova, T.V., Reynolds, I.J., 2003. Spontaneous changes in mitochondrial membrane potential in single isolated brain mitochondria. Biophys. J. 85, 3358–3366.

Vergun, O., Votyakova, T.V., Reynolds, I.J., 2004. Studies of single isolated mitochondria reveal different properties of Ca^{2+}-induced depolarization in brain and liver mitochondria. Biophys. J. 86 (1), 506A.

Wagner, J., Keizer, J., 1994. Effects of rapid buffers on Ca^{2+} diffusion and Ca^{2+} oscillations. Biophys. J. 67, 447–456.

Westerhoff, H.V., van Echteld, C.J.A., Jeneson, J.A.L., 1995. On the expected relationship between Gibbs eneergy of ATP hydrolysis and muscle performance. Biophys. Chem. 54, 137–142.

Wingrove, D.E., Gunter, T.E., 1986. Kinetics of mitochondrial calcium transport. II. A kinetic description of the sodium-dependent calcium efflux mechanism of liver mitochondria and inhibition by ruthenium red and by tetraphenylphosphonium. J. Biol. Chem. 261, 15166–15171.